REPORT DOCUMENTATION PAGE

1. REPORT DATE *(DD-MM-YYYY)*	2. REPORT TYPE	3. DATES COVERED *(From - To)*

4. TITLE AND SUBTITLE

5a. CONTRACT NUMBER

5b. GRANT NUMBER

5c. PROGRAM ELEMENT NUMBER

6. AUTHOR(S)

5d. PROJECT NUMBER

5e. TASK NUMBER

5f. WORK UNIT NUMBER

7. PERFORMING ORGANIZATION NAME(S) AND ADDRESS(ES)

8. PERFORMING ORGANIZATION REPORT NUMBER

9. SPONSORING / MONITORING AGENCY NAME(S) AND ADDRESS(ES)

10. SPONSOR/MONITOR'S ACRONYM(S)

11. SPONSOR/MONITOR'S REPORT NUMBER(S)

12. DISTRIBUTION / AVAILABILITY STATEMENT

13. SUPPLEMENTARY NOTES

14. ABSTRACT

15. SUBJECT TERMS

16. SECURITY CLASSIFICATION OF:			17. LIMITATION OF ABSTRACT	18. NUMBER OF PAGES	19a. NAME OF RESPONSIBLE PERSON
a. REPORT	b. ABSTRACT	c. THIS PAGE			19b. TELEPHONE NUMBER *(include area code)*

Standard Form 298 (Rev. 8-98)
Prescribed by ANSI Std. Z39.18
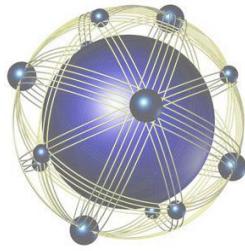
High Performance Technologies Inc.
11440 Commerce Park Drive, Suite 600
Reston, VA 20191

Blast Fragmentation Modeling and Analysis
BY09-005SP
Deliverable 03

Final Paper to the 27th Army Research Conference

Submitted by
Mary J. Graham
31 October 2010

for
User Productivity Enhancement, Technology Transfer, and Training (PETTT) Program

High Performance Computing Modernization Program (HPCMP)

Contract No.: GS04T09DBC0017

Government Users/Sponsors/Partners: Stephen Bilyk (RDRL/WMT-D)

BLAST FRAGMENTATION MODELING AND ANALYSIS

M. J. Graham
High Performance Technologies, Inc.
Reston, VA 20190

S. R. Bilyk
Army Research Laboratory
Aberdeen Proving Ground, MD 21005

ABSTRACT

Explosively driven fragmentation of ductile materials has long been a subject of great interest in both the design of munitions and armaments and the importance of reducing the vulnerability and enhancing the lethality of armor systems and personnel, Gurney, 1943; Taylor, 1963. The objective of this research is to develop a methodology to quantify and characterize near-field fragmentation from a multi-mode weapons device containing a multiphase blast explosive (MBX).

1. INTRODUCTION

The ARL Survivability Lethality and Analysis Directorate (SLAD) is seeking to develop a fast running lethality model that incorporates the combined lethality contributions of both blast and fragments from a Small Diameter Bomb (SDB) at close standoff. SLAD engineers have teamed with researchers from the ARL Weapons and Materials Research Directorate (WMRD) to bridge some of the gaps encountered between high fidelity continuum modeling and fast analytical survivability tools. Our approach is to model a series of exploding steel cylinder experiments designed to determine the fracture strains and the failure mechanisms caused by the passage of a strong shock. They include casing material, high explosive (HE) fill and detonator. The numerical results are compared with experimental data for predictive accuracy. The results of the two-dimensional (2D) and three-dimensional (3D) calculations and comparisons with data are presented. Analysis of the dynamic expansion and subsequent breakup of the casing shows that an engineering based failure model with statistical distributions coupled with void material seeding is sufficient to characterize warhead case fragmentation and merits continuation of sensitivity studies for validation and verification purposes to quantify the near field effects.

2. EXPERIMENTAL CONFIGURATION

The experiments modeled in this paper were designed to examine the dynamic expansion of explosively driven material to fragmentation, Goto, et al., 2008. The case has an axisymmetric cylindrical geometry and is fabricated from AerMet 100 alloy and AISI 1018 steel. It is loaded with a high explosive main charge, LX 17, top-initiated by an LX 10 frustum booster with RP 1 detonator. The detonation wave inside the cylinder provides a pressure front on the order of 10's of GPa. This intense wave leads to shock formation in the material with strain rates between 10^4 s^{-1} and 10^5 s^{-1}, conditions known to produce a state in which the material fails.

The experiments were performed with either high speed diagnostics or material soft-capture using a steel cylinder. The high-speed diagnostics are fast framing cameras, flash radiography and velocity history at the outside surface of the material. The experimental configuration is shown in Fig. 1. The metal rings, shown in Fig. 1. (b), were used to aid in the recovery of material fragments to investigate stress-state effects.
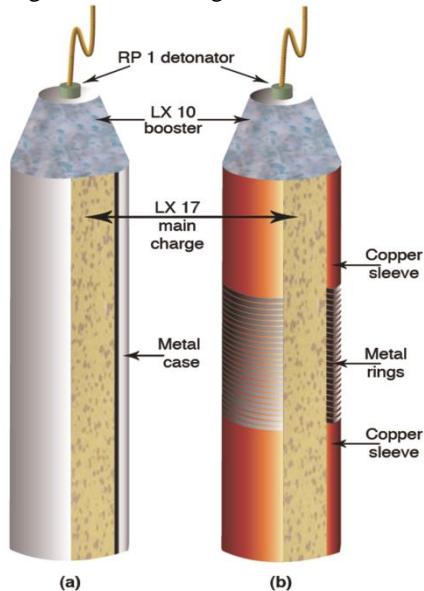

Fig. 1. Schematic of LX-17 doped (a) steel cylinder and (b) steel rings, Goto, et al., 2008.

The stacking of metal rings aids in the investigation of uniaxial stress loading and improves the statistics of the fragment recovery. This ringed configuration was performed in a soft capture tank and is shown in Fig. 2. (a). Some of the recovered fragments are shown in Fig. 2. (b).
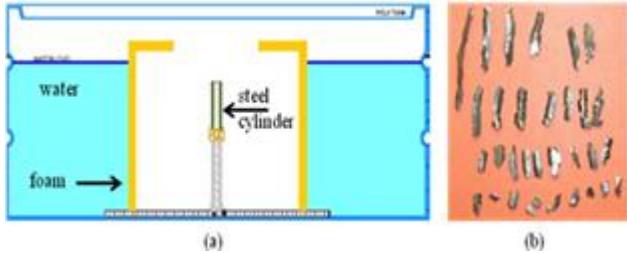

Fig. 2. (a) Schematic of recovery tank used for ringed geometry of a steel sample, and (b) recovered fragments, Goto, et al., 2008.

High speed diagnostics were not included in the second set. Our numerical predictions were directly compared with observed optical imagery and velocimetry data for the purposes of calibration, validation and benchmarking of the numerical model. Preliminary comparisons with statistical analysis from fragment recovery will also be discussed below.

3. METHOD OF SOLUTION

Numerical challenges are encountered to obtain quantitative information for a blast loaded fragmentation field. For a pure Lagrangian simulation, hourglassing will eventually lock highly distorted element regions and drive down the timestep. On the opposite end of the spectrum for a pure Eulerian simulation, material advection will eventually smear or nullify fragment material and therefore lose information on fragment mass and velocity. In order to simulate the highly complex phenomenon, the exploding cylinder is modeled with the hydrodynamics code ALE3D, an arbitrary Lagrangian-Eulerian multiphysics code, developed at Lawrence Livermore National Laboratory. ALE3D includes physical properties, constitutive models for the deviatoric and volumetric response as well as a fracture model with a statistical distribution to represent void nucleation, growth and coalescence and a newly developed seeding algorithm for fracture surface creation, Becker, 2010. ALE3D is used in Lagrangian mode with advection to address mesh distortion and tangling. The code is used in both two- and three-dimensions (2D, 3D, respectively). ALE3D in 2D does not resolve the fracturing of the cylinder, but it does provide details of the dynamics involved with shock formation, passage through the cylinder, compression and

tension produced in the metal along with a continuous history of the associated stress and strain in the material and velocity of the outer surface of the steel. Using the code in 2D provides rapid turnaround for parameter sweeps and sensitivity studies.

A Mie-Gruneisen equation of state is used to model the physical properties. The yield strength, Y, is given by the Steinberg-Guinan model, allowing for strain rate dependence. The basic model is described in Steinberg, 1991. The yield strength in terms of equivalent plastic strain, $\bar{\varepsilon}_p$, equivalent plastic strain rate, $\dot{\bar{\varepsilon}}_p$, pressure, P, and temperature,.
T, is given by

$$Y = Y_0 f\left(\bar{\varepsilon}_p, \dot{\bar{\varepsilon}}_p\right) \frac{G(P,T)}{G_0} . \qquad (1)$$

The form of the shear modus, G, has linear dependence on the normalized pressure and temperature, and is given, in general, by,

$$G = \left[G_0 + a_p G_0 P \left(1 - a_n + a_n \eta^{-1/2}\right) - G_0 a_T (T - T_{\text{ref}})\right] \exp\left(-\frac{a_M E}{E_m - E}\right), \qquad (2)$$

where $\eta \equiv \rho/\rho_0$. The initial yield, Y_0, is given by

$$Y_0 f\left(\bar{\varepsilon}_p, \dot{\bar{\varepsilon}}_p\right) = Y_0 \left[1 + \beta\left(\bar{\varepsilon}_p + \varepsilon_0\right)\right]^n \left[a + b\dot{\bar{\varepsilon}}_p\right]^m \leq Y_{max} \qquad (3)$$

where G_0 is the initial shear modulus, a_p and a_n are the pressure dependence and relative volume dependence of G, respectively; a_T and a_M are the linear temperature dependent and coefficient adjusting the melt-softening of G; ρ and ρ_0 are the density and initial density, respectively. In this case, we specify the Poisson ratio, and therefore, the Young's modulus, E, is set to zero, thus eliminating the exponential. In the equation for the initial yield, β is a work hardening parameter, a and b are additive rate-dependent and strain rate normalization constants, respectively, n and m are work hardening and rate sensitivity exponents, respectively, and ε_0 is strain offset.

Since fragmentation is inherently a 3D event, additional modeling is essential for more accurate representation. A schematic of the evolution of the fragmentation process of the steel cylinder is demonstrated in Fig. 3. The initial blast pushes radially against the inner cylindrical wall and forms a compressive wave inside the material, as shown in Fig. 3 (a). As the

compression wave reaches the outer diameter (OD), it reflects at the free surface and puts the material in tension, creating spall along the circumference toward the OD. In Fig. 3 (b) the OD of pressure-containing ring is in tension, emanating radial brittle cracks from the spall ring. Eventually, shear cracks form and carry the failure through the compressive region, as in Fig. 3 (c).

The typical process for fracture is void nucleation, growth of the void, void coalescence and fracture surface creation, Hertzberg, 1996. In the ALE3D simulations we are not predicting nucleation but are inserting voids into the casing material. With limited knowledge of the


| (a) | (b) | (c) |
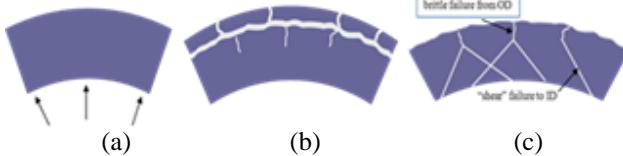
Fig. 3. Schematic of the fragmentation process. (a) Initial pressure blast, (b) OD of ring starting brittle cracks, (c) failure is carried through the compressive region.

nucleation to growth process (below the continuum length scale), some model developers take the approach of void seeding. In this study the Johnson-Cook (JC) fracture model, Johnson, 1985, is chosen for the case material, where the failure strain, ε_f, is given by,

$$\varepsilon_f = \left(\widehat{D}_0 + \widehat{D}_D \exp\left(D_3 \frac{p}{\bar{\sigma}}\right)\right)\left(1 + D_4 \ln\left(\frac{\dot{\varepsilon}}{\dot{\varepsilon}_0}\right)\right)(1 + D_5 T^*), \quad (4)$$

where $\widehat{D}_0$ and $\widehat{D}_D$ are coefficients in failure criterion, D_3 is a constant multiplying triaxiality, D_4 and D_5 are coefficients for log stain rate factor and for temperature factor, respectively, p and $\bar{\sigma}$ are pressure and current equivalent flow stress, respectively, and T^* is the normalized temperature. The failure/fracture model works in conjunction with the classical von Mises yield condition,

$$\bar{\sigma}_e = Y, \qquad \bar{\sigma}_e \equiv \sqrt{3J_2}, \qquad J_2 \equiv \frac{1}{2}\sigma'_{ij}\sigma'_{ij}, \quad (5)$$

where $\bar{\sigma}_e$ is the effective stress and σ'_{ij} is the deviatoric Cauchy stress.

According to the JC model, material failure occurs when the damage parameter, $D = \Sigma\left(\Delta\varepsilon_f/\varepsilon_f\right)$, reaches unity. For *mesh-independent* fragmentation simulations, the seeding of a distribution of defects (voids) into a failure model is essential, and the statistics of the defect

distribution govern the fragment size and mass distribution, Becker, 2010. In keeping with the analysis used by Goto, et al., 2008, a Weibull probability distribution function is used to seed the voids,

$$f(t) = \left(\frac{\beta}{\eta}\right)\left(\frac{t-\gamma}{\eta}\right)^{\beta-1}\exp\left[-\left(\frac{t-\beta}{\eta}\right)^{\beta}\right], \quad (6)$$

where β and η are a shape factor and γ is a location parameter required to define a critical strain below which there is a zero probability the material will fail. For the JC fracture model, the function is placed in the monotonic term describing stress triaxiality specifically, as a multiplier to $\widehat{D}_0$. In addition, controlled mixed cell algorithm was added to ALE3D which prevents mesh tangling and allows product gases to vent through failed casing material, Becker 2010.

The ALE3D simulation of the evolution of the fragmentation process is shown in Fig. 4. Fig. 4 contains the pressure history of the explosive material and the failure history of the steel cylinder. In Fig. 4 (a) the high pressure front from the detonation wave has reached the inner surface of the case material. Within 2.5 μs, the pressure front has compressed the steel, reflected off the OD, placing the material in tension. As the diameter is expanded due to blast loading, regions of failure can be seen in the material (see Fig. 4 (b)). 10.0 μs after the detonation wave loads the inner casing material, failure is detected within the compressive region. Fig. 4 (c) shows regions of failure that have formed from the outer to inner diameters after the reflected tensile wave reached the inner surface. We note that without a Weibull function i.e. for a constant $\widehat{D}_0$, failure would occur throughout the entire thickness of the steel casing. Additionally, we emphasize that the JC failure model is engineering based, has difficulty calibrating the triaxiality parameter, lacks flaw orientation, and obtaining the functional form for the failure distribution can be application dependent. Even with these limitations, as will be discussed in the next section, surprisingly good results are obtained from 2D and 3D numerical simulations when compared with experiment.


| (a) | (b) | (c) |
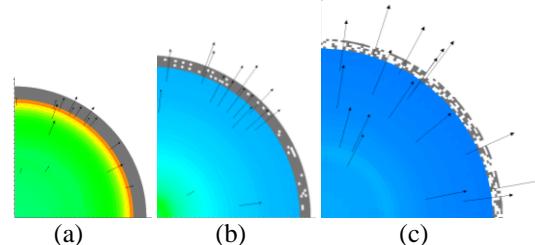
Fig. 4. ALE3D simulation of fragmentation process. (a) Detonation wave reaches inner surface of steel cylinder,

(b) material failure interior to steel case after reflection, (c) material failure formed through cylinder.

4. RESULTS

The ALE3D initial configuration for the 2D and 3D calculations are shown in Fig. 5(a) and (b), respectively. All simulations were run on the HPC ARL DSRC Linux Networx cluster, MJM, using 128 processors for approximately 10 hours.
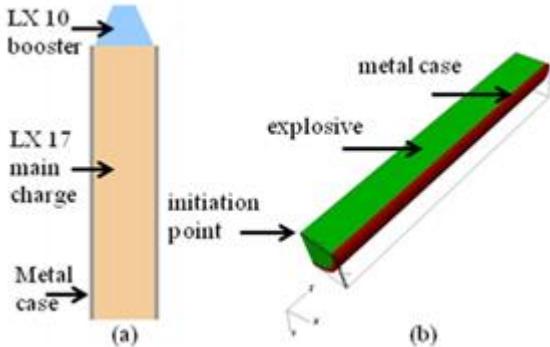

Fig. 5 (a) Schematic for 2D calculation and (b) 3D calculation.

For the 2D simulations, the HE booster is detonated at the center-point of the cylinder. The Jones-Wilkins-Lee (JWL) equation of state is used to describe the pressure-volume-energy behavior of the detonation products of both the LX 10 (booster) and the LX 17 (main charge), Kury, 1965. The JWL equation of state is given by

$$p = A\left(1 - \frac{\omega}{R_1 V}\right)\exp(-R_1 V)$$
$$+ B\left(1 - \frac{\omega}{R_2 V}\right)\exp(-R_2 V) + \frac{\omega}{V}E, (7)$$

where E is the material energy and V is the relative volume. The material dependent parameters A, B (linear coefficients) and R_1, R_2, ω (nonlinear coefficients) are provided by LLNL Explosives Handbook, LLNL, 1985.

As the high explosive shock traverses the cylinder, radial deformation takes place (for 2D only). The calculation allows evaluation of the time dependent pressure, density and material properties as the shock front propagates. The evolution of the deformation of the cylinder and passage of the wave is shown at 10 μs and 22 μs in Fig. 6 (a) and Fig. 6 (b), respectively. A closer zoom at the cylinder wall in the vicinity of the shock shows that a pressure wave reverberates in the cylinder against the inner and outer walls (see Fig, 6 (b) first inset). The peak pressure is approximately 26 GPA and decreases to zero at later time. Finally, the pressure

asymptotes to approximately -500 MPa, i.e., 500 MPa tensile, setting the stage for failure, fracture and fragmentation. The density of the cylinder starts at 7.8 g/cm^3 and reaches a peak value of 8.6 g/cm^3 at the shock front (see Fig. 6 (b) second inset).

The 3D calculations were not modeled with the booster. The main charge, LX 17, was point detonated at the top of the configuration at the center of the main charge. The pressure history for the high explosive and steel from the 3D calculation is shown in Figs. 7(a) and (b) at 5 μs and 15 μs, respectively, after detonation, where the shock front is nearly planar (Fig 7(b)). The oscillatory
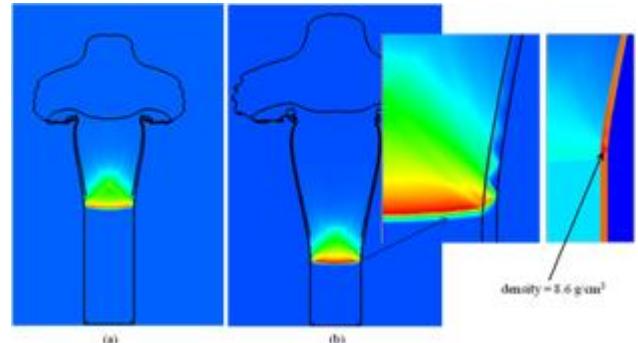

Fig. 6. 2D numerical results of wave front and cylinder expansion at (a) 10 μs after detonation and (b) 22 μs after detonation.

behavior of the shock in the material is demonstrated in Fig. 7 inset, which appear as pressure rings inside the material. The peak pressure is approximately 28 GPa and the peak density is approximately 8.9 g/cm^3. Both peaks are nearly the same as obtained from 2D calculation.
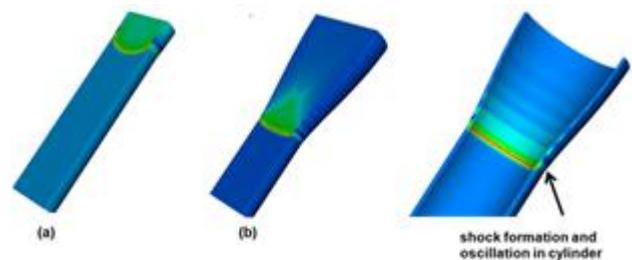

Fig. 7 Evolution of wave front in high explosive and steel, pressure profile (a) 5 μs after detonation (b) 10 μs after detonation, and inset showing steel case only.

The velocity of the expanding material was measured at several locations along the length of the cylinder. The measured (solid curve) and calculated (dashed curve) velocity history are shown in Fig. 8. Overestimates in the calculated velocity are seen at approximately 28 and 29 μs. It is believed that the discrepancy (about 10 percent)

is due to the frequency in sampling in the calculation versus the observed sample window. We note that for several experiments in this series, the measured velocity spiked similar to the predicted in Fig. 8, Goto, 2010. The measured velocity asymptotes at approximately 1700 m/s are somewhat higher than the calculation, 1610 m/s. The disagreement in the magnitude of the velocity can be due to the strength of the material retarding the expansion, especially in view of the fact that the material has failed at the location of the velocity probe, approximately 32.5 μs.
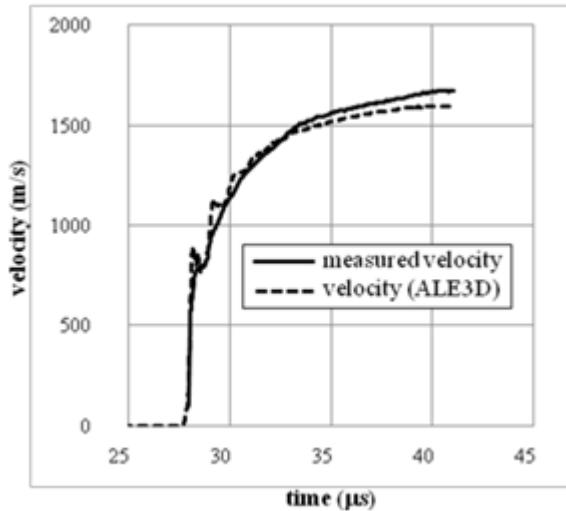

Fig. 8.   Measured and calculated cylinder expansion velocity (m/s) versus time (μs).

The ALE3D calculations performed in 3D were compared with the high speed diagnostics, in particular the optical images, along with the through thickness strain, defined as,

$$\varepsilon_{tt} = ln\left(\frac{t_{final}}{t_{initial}}\right), \tag{8}$$

where t_{final} and $t_{initial}$ are the final and initial thicknesses of the material, respectively. The optical image shown in Fig. 9 (a) (25 μs after detonation) contains three markers, 0.15, 0.20 and 0.30, that indicate different regions of circumferential strain. When compared to the through-thickness strain the optical markers correspond to expanding diameters namely, 5.93 cm, 6.21 cm and 6.86 cm, respectively. These locations were chosen because the image shows changes in the texture associated with the entire history of the deformation: (1) expanded material, (2) expanded material with cracking, and (3) failed material.

The ALE3D calculation provided in Fig. 9 (b) shows the same features in the evolution of the deformation.

The calculated diameters where expansion, cracking and failure occurred were 6.20 cm, 6.8 cm, and 7.4 cm. The numerical results over predict those obtained from the optical imagery however, the results are within 10 percent. For our applications, this is considered to be in good agreement with experiment.

While the agreement in the expanded (no failure) and fragmented regions is good, the region where void nucleation, growth and coalescence occur is higher than expected. It is believed that the disagreement in the mid region may be due to the statistical damage model used governing the size and distribution of the voids. We are currently performing a sensitivity study of the parameters that control the functional form of the Weibull distribution as a means to reconcile the difference in the calculated diameter.


(a)   (b)
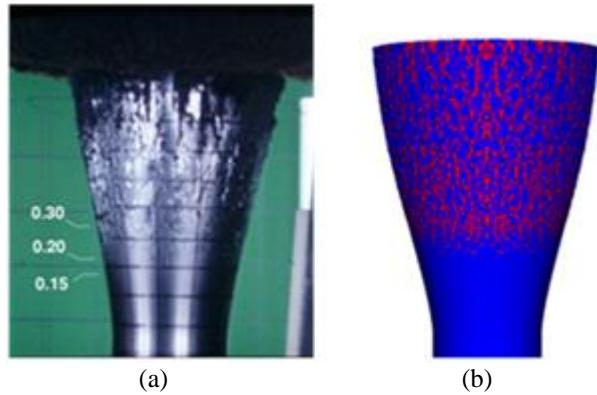
Fig. 9. History of deformation: expansion, cracking and failure of cylinder, (a) Optical image 25 μs after detonation, Goto, et al., 2008, (b) ALE3D simulation.

The evolution of the exploding cylinder from the ALE3D calculation is shown in Fig. 10. Intact material is shown in gray in Frames (i) – (iii) and the initial state is superimposed with the profile of the mass of the cylinder
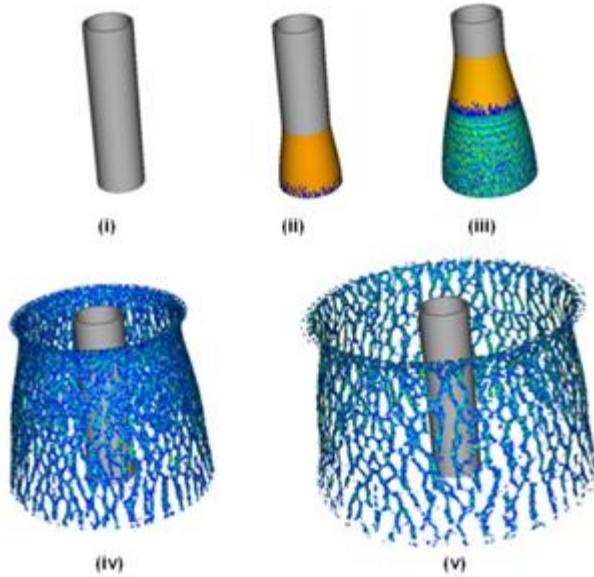
Fig. 10 Deformation of the steel cylinder from the ALE3D calculation (explosive not shown). Evolution of cylinder mass superimposed. (i) Steel cylinder at time = 0, (ii) Time = 10 μs after detonation, (iii) Time = 20 μs, (iv) Time = 50 μs (time = 0 μs in gray), and (v) Time = 70 μs.

in Frames (iv) and (v) of Fig. 10. Approximately 20 μs after the detonation of the high explosive, the texture of the steel cylinder has changed, and some cracks are visible to the naked eye. However, analysis with the current fragment field finder shows that fragmentation occurs at approximately 12 μs after detonation. By 25 μs, the detonation wave has traversed the length of the steel cylinder (shortly after Frame (iii)). Subsequent frames show a slight flare at the top of the cylinder. This is due to the symmetry boundary condition and does not affect the analysis of the fragments. The radial motion continues until the calculation reaches the computational boundary, which is located at the same radial distance as the foam in the soft recovery tank.

At the near field, the fragments are long jagged strips that are further broken apart into smaller pieces as they travel with air drag into the far field. Fig. 11 (a) and (b) shows the evolution of the mass of the cylinder at 42.5 and 62.5 μs after detonation, respectively. As the radial distance of the cylinder increases, the number of fragments (connected components) increases by a factor of three.
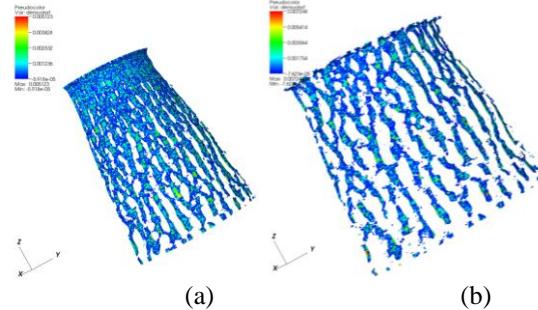

Fig. 11. Mass of the fragment field during evolution of the fragmentation of the cylinder. As the radial distance increases, the number of fragments (connected components) increases.

Analysis of the numerical results continues. We are currently studying the thinning of the cylinder wall at numerous locations and calculated equivalent plastic strain from the numerical simulations to determine shock induced strain. Further comparisons with the soft capture analysis from the experiment will also continue as data becomes available. In addition, we are also cooperatively working with computer scientists from the ARL Computational and Information Sciences Directorate (CISD) to develop software that will collect post-processed output from ALE3D and translate it into format suitable for use as a near-field fragmentation database for SLAD lethality analysis.

CONCLUSIONS

Comparisons of numerical predictions with observed data show good agreement and the modeling demonstrates anticipated trends. Continued analysis is warranted for validation, verification and benchmarking of the code features and constitutive models used for this application. The agreement with the experimental data is quite good, and therefore, modification of the fragment finder post-processing software will move forward to meet the goals for building a database of fragment size and velocity in the near field. Analysis of the dynamic expansion and subsequent breakup of the casing shows that using an engineering based failure model with statistical distributions coupled with void material seeding is sufficient to characterize warhead case fragmentation.

Current research includes performing 2D and 3D numerical simulations for blast fragmentation using a multiphase explosive for sensitivity analysis and blast/fragmentation statistical analysis.

REFERENCES

Becker, R., 2010 (private communications).

Goto, D.M., Becker, R., Orzechowski, T.J., et al., 2008: Investigation of the Fracture and Fragmentation of Explosively Driven Rings and Cylinders, *Int. J. Impact Eng.*, **35**, Issue 12, 1547-1556.

Goto, D.M., 2010 (private communications).

Gurney, R. W., 1943: The Initial Velocity of Fragments from Bombs, Shells and Grenades, Army Ballistics Research Laboratory Report No. 405.

Hertzberg, R., 1996: Deformation and Fracture Mechanics of Engineering Materials, Wiley and Sons, Inc., 4th ed.

Johnson, G.R., and Cook, W.H., et al., 1985: Fracture Characteristics of Three Metals Subject to Various Strains, Strain Rates, Temperatures and Pressures, *Eng. Frac. Mech*, **21**(1): 31-48.

Kury, J.W., Hornig, H.C., Lee, E.L., et al., 1965: Metal acceleration by chemical Explosives. *Fourth Int. Det. Symp.,* Office of Naval Research, ACR-126, 3-13.

LLNL, 1985: LLNL Explosives Handbook, Properties of Chemical Explosives and Explosive Simulants.
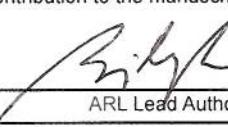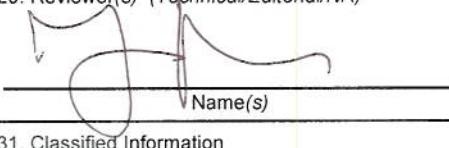
Steinberg, D. J., et al., 1991: Equation of State and Strength Properties of Selected Materials, UCRL-MA-106439.

Taylor, G. I., 1963: Analysis of the Explosion of a Long Cylindrical Bomb Detonated at One End, Scientific Papers of G. I. Taylor, vol. III, Cambridge University Press, No. 30, 277-286.

Quality Assurance and OPSEC Review

7979

This form is an approval record for ARL generated information to be presented or disseminated external to ARL. Note: Submit all manuscripts in electronic format or camera ready copy. See attached instructions. If more space is needed, use reverse of form *(include block numbers)*.

A. General Information	1. Present Date	2. Unclassified Title
	09/21/2010	Blast Fragmentation Modeling and Analysis

3. Author(s)	4. Office Symbol(s)	5. Telephone Nr(s)
Mary Jane Graham, HPTi and Stephan R. Bilyk, ARL	RDRL-WMP-B	410-278-2976

6. Contractor generated ☐ No ☒ Yes
If yes, enter Contract No. and ARL COR
GS04T09DBC0017 and BY09-005SP.
Signed CRADA between HPTi and ARL.

7. Type: ☐ Report ☐ Abstract ☒ Publication ☐ Presentation *(speech, briefing, video clip, poster, etc)* ☐ Book ☐ Book Chapter ☐ Web

8. Key Words
fragmentation, void seeding

9. Distribution Statement *(required)* Is manuscript subject to export control? ☒ No ☐ Yes

Circle appropriate letter and number. *(see instructions for statement text)*
☒ B C D E F X 1 2 3 4 5 6 7 8 9 10 11

10. Security Classification
UNCL

B. Reports	11. Series	12. Type	13. No. of pages	14. Project No.	15. Period Covered	16. Sponsor

C. Publications

17. Is MS an invited paper? ☒ No ☐ Yes

18. Publication is a refereed journal? ☒ No ☐ Yes

19. Material will be submitted for publication in

Conference Proceedings
_____
Journal

US
_____
Country

D. Presentations	20. Conference Name/Location	21. Sponsor
	27th Army Science Conference/Orlando, FL	Asst. Sec. Army (Acq., Log., & Tech.)

22. Conference Date	23. Due Date	24. Conference is
11/29/2010	09/22/2010	☐ Open to general public ☒ Unclassified/controlled access ☐ Classified

25. For nonpublic meetings: Will foreign nationals be attending?
☐ No ☐ Yes *(If yes, list countries and identify International Agreement(s))*
☒ Don't know

26. Material will be
☐ Oral presented only ☐ Oral presented and published in

(If published, complete block 18 and 19, Section C.)

E. Authors Statement: 27. All authors have concurred in the technical content and the sequence of authors. All authors have made a substantial contribution to the manuscript and all authors who have made a substantial contribution are identified in Block 3.

_____
ARL Lead Author or COR

21 SEP 10
Date

F. Approvals

28. First line Supervisor of Senior ARL Author or COR
Christopher Hoppel 9/22/10
Name   Date

29. Reviewer(s) *(Technical/Editorial/NA)*

_____
Name(s)

9/22/2010
Date

30. Limited distribution information for release to foreign nationals

31. Classified Information

Classified by _____

Declassified on _____

_____
Foreign Disclosure   Date

_____
Command Security Manager   Date

OPSEC REVIEW CHECKLIST

OPSEC POC: Complete and explain any positive responses in block 9.
Note: ARL must be the proponent of the proposed information for release.

1. Does this material contain Sensitive Information? ☐ YES ☒ NO

2. Does this information contain state-of-the-art, breakthrough technology? ☒ YES ☐ NO

3. Does the United States hold a significant lead time in this technology? ☒ YES ☐ NO

4. Does this information reveal aspects of reverse engineering? ☐ YES ☒ NO

5. Does this material reveal any security practices or procedures? ☐ YES ☒ NO

6. Does this information reveal any security practices or procedures? ☐ YES ☒ NO

7. Would release of this information be of economic benefit to a foreign entity, adversary, or allow for the development of countermeasures to the system or technology? ☐ YES ☒ NO

8. Does this material contain:

a. Any contract proposals, bids, and/or proprietary information? ☐ YES ☒ NO

b. Any information on inventions/patent application for which patent secrecy orders have been issued? ☐ YES ☒ NO

c. Any weapon systems/component test results? ☐ YES ☒ NO

d. Any ARL-originated studies or after action reports containing advice and recommendations? ☐ YES ☒ NO

e. Weakness and/or vulnerability information? ☐ YES ☒ NO

f. Any information on countermeasures? ☐ YES ☒ NO

g. Any fielding/test schedule information? ☐ YES ☒ NO

h. Any Force Protection, Homeland Defense *(security)* information? ☐ YES ☒ NO

i. Information on subjects of potential controversy among military services or other federal agencies? ☐ YES ☒ NO

j. Information on military applications in space, nuclear chemical or biological efforts: high energy laser information; particle beam technology; etc? ☐ YES ☒ NO

k. Contain information with foreign policy or foreign relations implications? ☐ YES ☒ NO

OPSEC Approval Statement

I, the undersigned, am aware of the adversary's interest in DOD publications and in the subject matter of this material and that, to the best of my knowledge, the net benefit of this release out weights the potential damage to the essential security of all ARL, AMC, Army, or other DOD programs of which I am aware.

JOHN CLAYTON   _(signature)_   22 Sept 2010

OPSEC Reviewer *(Printed name/signature)*   Date

9. Space for explanations/continuations/OPSEC review comments

U.S. lead in technology for fragment simulations (LLNL and ARL).
No information regarding lethality is revealed.

Final Release Clearances

32. Public/~~Limited~~ release information

a. Material has been reviewed for OPSEC policy.

Erich W. Meyerhoff   9/23/10

ARL OPSEC Officer   Date

b. The information contained in this material is ☒ / is not ☐ approved for public release/ has received appropriate tech/editorial review.

Todd Byrd for Pat Baker   23 Sep 2010

Division Chief   Date

c. This information is accepted for public release.

Erich W. Meyerhoff   9/23/10
for

Public Affairs Office   Date